Zurich Open Repository and Archive
University of Zurich
University Library
Strickhofstrasse 39
CH-8057 Zurich
www.zora.uzh.ch

Year: 2019

A New Zebrafish Model for CACNA2D4-Dysfunction

Schlegel, Domino K ; Glasauer, Stella M K ; Mateos, José M ; Barmettler, Gery ; Ziegler, Urs ; Neuhauss, Stephan C F

Abstract: Purpose Mutations in CACNA2D4, encoding the 2 4 subunit of retinal voltage-gated calcium channels (Cav), cause a rare type of retinal dysfunction in human, mainly affecting cone vision. Here, we investigate the role of CACNA2D4 in targeting of Cav, its influence on cone-mediated signal transmission, and the cellular and subcellular changes upon loss of 2 4 by exploiting the advantages of the cone-dominant zebrafish as model system. Methods We identified two zebrafish CACNA2D4 paralogs (cacna2d4a and cacna2d4b), analyzed their expression by RNA in situ hybridization and introduced truncating frameshift mutations through CRISPR/Cas9-mediated mutagenesis. We analyzed retinal function and morphology of the single and double mutant lines by electroretinography, immunohistochemistry, light- and electron microscopy. Results Knockout of cacna2d4b reduces the expression of Cacna1fa, the pore-forming subunit of retinal Cav1.4, whereas loss of cacna2d4a did not. Only knockout of both paralogs impaired cone-mediated ERG b-wave amplitude. The number of "floating" ribbons is increased in double-KO, while retinal morphology and expression of postsynaptic mGluR6b remain largely unaffected. Both Cacna1fa and Ribeyeb show ectopic punctate expression in cacna2d4b-KO and double-KO photoreceptors. Conclusions We find that increasing the expression of Cav at the synaptic membrane is an evolutionarily conserved function of Cacna2d4b. Yet, since both paralogs participate in cone synaptic transmission, we propose partial subfunctionalization in zebrafish. Similar to human patients, our double KO zebrafish model shows mild cone dysfunction, which was not associated with signs of retinal degeneration. Therefore, cacna2d4-KO zebrafish is a suitable model to study the pathophysiological mechanisms underlying CACNA2D4 dysfunction in human.

DOI: https://doi.org/10.1167/iovs.19-26759

Posted at the Zurich Open Repository and Archive, University of Zurich
ZORA URL: https://doi.org/10.5167/uzh-182385
Journal Article
Published Version

The following work is licensed under a Creative Commons: Attribution-NonCommercial-NoDerivatives 4.0 International (CC BY-NC-ND 4.0) License.

Originally published at:
Schlegel, Domino K; Glasauer, Stella M K; Mateos, José M; Barmettler, Gery; Ziegler, Urs; Neuhauss, Stephan C F (2019). A New Zebrafish Model for CACNA2D4-Dysfunction. Investigative Ophthalmology Visual Science [IOVS], 60(15):5124-5135.
DOI: https://doi.org/10.1167/iovs.19-26759

A New Zebrafish Model for CACNA2D4-Dysfunction

Domino K. Schlegel,[1,2] Stella M. K. Glasauer,[1,3,4] José M. Mateos,[5] Gery Barmettler,[5] Urs Ziegler,[5] and Stephan C. F. Neuhauss[1]

[1]Institute of Molecular Life Sciences, University of Zurich, Zurich, Switzerland
[2]Life Science Zurich Graduate School, Ph.D. Program in Molecular Life Sciences, Zurich, Switzerland
[3]Neuroscience Research Institute, University of California, Santa Barbara, Santa Barbara, California, United States
[4]Department of Molecular, Cellular, and Developmental Biology, University of California, Santa Barbara, Santa Barbara, California, United States
[5]Center for Microscopy and Image Analysis, University of Zurich, Zurich, Switzerland

Correspondence: Stephan C. F. Neuhauss, Institute of Molecular Life Sciences, University of Zurich, Winterthurerstrasse 190, Zurich, CH-8057, Switzerland; stephan.neuhauss@imls.uzh.ch.

DKS and SMKG contributed equally to work presented here and should therefore be regarded as equivalent authors.

Submitted: January 28, 2019
Accepted: October 26, 2019

Citation: Schlegel DK, Glasauer SMK, Mateos JM, Barmettler G, Ziegler U, Neuhauss SCF. A new zebrafish model for CACNA2D4-dysfunction. *Invest Ophthalmol Vis Sci*. 2019;60:5124–5135. https://doi.org/10.1167/iovs.19-26759

Purpose. Mutations in *CACNA2D4*, encoding the $\alpha_2\delta_4$ subunit of retinal voltage-gated calcium channels (Ca_v), cause a rare type of retinal dysfunction in human, mainly affecting cone vision. Here, we investigate the role of CACNA2D4 in targeting of Ca_v, its influence on cone-mediated signal transmission, and the cellular and subcellular changes upon loss of $\alpha_2\delta_4$ by exploiting the advantages of the cone-dominant zebrafish as model system.

Methods. We identified two zebrafish *CACNA2D4* paralogs (*cacna2d4a* and *cacna2d4b),* analyzed their expression by RNA in situ hybridization and introduced truncating frameshift mutations through CRISPR/Cas9-mediated mutagenesis. We analyzed retinal function and morphology of the single and double mutant lines by electroretinography, immunohistochemistry, light- and electron microscopy.

Results. Knockout of *cacna2d4b* reduces the expression of Cacna1fa, the pore-forming subunit of retinal $Ca_v1.4$, whereas loss of *cacna2d4a* did not. Only knockout of both paralogs impaired cone-mediated ERG b-wave amplitude. The number of "floating" ribbons is increased in double-KO, while retinal morphology and expression of postsynaptic mGluR6b remain largely unaffected. Both Cacna1fa and Ribeyeb show ectopic punctate expression in *cacna2d4b*-KO and double-KO photoreceptors.

Conclusions. We find that increasing the expression of Ca_v at the synaptic membrane is an evolutionarily conserved function of Cacna2d4b. Yet, since both paralogs participate in cone synaptic transmission, we propose partial subfunctionalization in zebrafish. Similar to human patients, our double KO zebrafish model shows mild cone dysfunction, which was not associated with signs of retinal degeneration. Therefore, *cacna2d4*-KO zebrafish is a suitable model to study the pathophysiological mechanisms underlying CACNA2D4 dysfunction in human.

Keywords: calcium channel, cone photoreceptor, zebrafish, disease model

Photoreceptors rely on specialized ribbon synapses for graded signal transmission over a wide range of stimulus intensities. Exocytosis at these ribbon synapses is mediated by the L-type high voltage-gated calcium channel $Ca_v1.4$,[1–4] which opens upon membrane depolarization of the photoreceptor cell in darkness, thereby allowing calcium-dependent glutamate release. Similar to other Ca_v, $Ca_v1.4$ are heteromultimeric protein complexes consisting of the pore-forming α_1F subunit, encoded by *CACNA1F*,[1,2] and auxiliary β and $\alpha_2\delta$ subunits. Although four different subtypes of each of the two auxiliary subunits exist that could potentially interact with α_1F, it has been suggested that β_2 and $\alpha_2\delta_4$, encoded by *CACNB2* and *CACNA2D4*, respectively, are the predominant subtypes in the photoreceptor synaptic terminal.[5–10]

The importance of α_1F is demonstrated in several studies on patients and animal models: *CACNA1F* mutations cause retinal disorders ranging from incomplete congenital stationary night blindness type 2,[1,2] cone-rod dystrophy[11–14] to Åland island eye disease.[15] In different model systems, α_1F has been proven important for signal transmission from photoreceptors to second order neurons and for ribbon synapse formation and maintenance.[1,2,16–20] The auxiliary β and $\alpha_2\delta$ subunits of Ca_v channels, have been reported to be involved in expression of the pore-forming subunit as well as in modulating the channel's biophysical properties (reviewed in Ref. 21). Mutations in *CACNA2D4* have been identified to cause a rare type of stationary or slowly progressive cone dysfunction[7,22] (Vincent A, et al. *IOVS* 2014;55:ARVO E-Abstract 6427). Patients present with mildly reduced visual acuity, impaired color vision, attenuated photopic ERG and photophobia, but show no signs for retinal degeneration[22] (Vincent A, et al. *IOVS* 2014;55:ARVO E-Abstract 6427), although one patient with foveal pigment mottling was reported.[7] Mice with a spontaneously occurring homozygous frameshift mutation in *Cacna2d4* show rod photoreceptor degeneration, thinning of the outer plexiform layer and a loss of both scotopic and photopic ERG responses.[6] Recent studies on two different *Cacna2d4*-KO mice suggest a role for Cacna2d4 in structural organization and function of rod[23,24] and cone synapses.[24] Interestingly, in all three studies, *Cacna2d4* mutation affects rods more severely than cones, and

Copyright 2019 The Authors

This work is licensed under a Creative Commons Attribution-NonCommercial-NoDerivatives 4.0 International License.

Downloaded from iovs.arvojournals.org on 12/16/2019

ERG revealed that both scotopic and photopic b-wave amplitudes are strongly reduced. Although these studies present a comprehensive model of Cacna2d4 affecting ribbon synapse structure and function in rods and partially in cones, it is not fully understood what causes the much milder and predominantly cone-specific phenotype in patients with *CACNA2D4* mutations.

The present study therefore focuses on the cone-specific aspects of Cacna2d4 function. We generated a complementary model for Cacna2d4-dysfunction by genome editing in the cone-dominant zebrafish. We show that $\alpha_2\delta_4$ is essential for expression and localization of $Ca_v1.4$ channels at photoreceptor synaptic terminals and conclude that this is an evolutionarily conserved function of the protein. Our model recapitulates findings in human patients, in that signal transmission from cone photoreceptors is diminished, but not completely absent, and that overall retinal morphology and integrity of photoreceptor cells is maintained over time.

Methods

Zebrafish Husbandry

Research was performed in accordance with the ARVO Statement for the Use of Animals in Ophthalmic and Vision Research and local authorities (Kantonales Veterinäramt TV4206). Zebrafish (Tü wild type strain) were kept at 26°C under a 14/10-hour light/dark cycle as described.[25] Embryos were raised at 28°C in E3 medium and staged according to development in days post fertilization (dpf).[26]

Bioinformatic Analysis of Cacna2d Family Members

Human and mouse Cacna2d proteins were used for Blast searches against the zebrafish genome assemblies zv9 and zv10 on Ensembl (www.ensembl.org; in the public domain). Predicted annotated proteins with similarity to mammalian Cacna2d proteins were ENSDARP00000096745, ENSDARP00000109719, ENSDARP00000132438, ENSDARP00000113230, ENSDARP00000001281, ENSDART00000136069, ENSDART00000048023, and ENSDARP00000006267. Phylogenetic analysis was performed on Phylogeny.fr.[27,28] Briefly, sequences were aligned with MUSCLE, ambiguous regions removed using Gblocks and conserved amino acids subjected to PhyML maximum likelihood phylogeny. The phylogenetic tree was rendered using TreeDyn. Proteins were analyzed for domains (SMART, http://smart.embl-heidelberg.de; in the public domain), signal peptides using (PrediSi, http://www.predisi.de/home.html; in the public domain), and omega sites and likelihood of GPI anchoring (PredGPI, http://gpcr.biocomp.unibo.it/predgpi; in the public domain).[29]

In Situ Hybridization

Fragments of *cacna2d4a* and *cacna2d4b* coding sequence were amplified from 5 dpf zebrafish cDNA with primers a1.1 and a1.2, or b1.1 and b1.2, respectively (Supplementary Table S2). PCR products were cloned into pCRII-TOPO (Invitrogen, Carlsbad, CA, USA) and plasmids were used for in vitro transcription of antisense and sense RNA probes with the Roche DIG-RNA Labeling Kit (Roche Diagnostics, Mannheim, Germany). Whole mount and section in-situ hybridization was carried out as described[30] with modifications.[31] Images were acquired on an Olympus BX61 microscope using DIC optics.

CRISPR/Cas9 Mutagenesis

CRISPR target sites of the GGN18 motif favorable for in-vitro transcription with T7 polymerase[32] were detected and oligonucleotides for cloning sgRNA templates (Supplementary Table S3) retrieved using ZIFIT (www.zifit.partners.org; in the public domain). Forward and reverse oligonucleotides were cloned into pT7-gRNA as described.[33] sgRNA template was amplified using primers sg1 and sg2 (Supplementary Table S2). sgRNAs were transcribed using the Megascript T7 kit (Ambion, Austin, TX, USA) and purified using the MEGAclear kit (Ambion).

Injection mixes (150 ng/µL sgRNA, 832 ng/µL Cas9-GFP[34] protein, 300 mM KCl) were incubated for 10 minutes at 37°C to allow formation of sgRNA/Cas9-GFP complexes.[35] Zygotes were injected with 1 nL injection mix. 10 pooled larvae per injected clutch were genotyped to verify efficient genome editing. Adult F0 fish were outcrossed to Tü wild type, and F1 offspring was analyzed for germline transmission by genotyping individual fin biopsies. Targeted regions of *cacna2d4a* (primers a2.1 and a2.2) and *cacna2d4b* (primers b2.1 and b2.2) were amplified (Supplementary Table S2), followed by cloning into pCRII-TOPO (Invitrogen) and plasmid sequencing. F1 fish with identical heterozygous frameshift mutations were crossed, and F2 generation were genotyped by amplification with primers a3.1, a3.2, b3.1, and b2.2 followed by restriction digest. In the *cacna2d4a* amplicon a3.1 introduces a mismatch generating an AluI restriction site in the wild type allele of *cacna2d4a*, while the wild type amplicon of *cacna2d4b* harbors an NlaIII restriction site that is lost upon mutation. Restricted PCR products were analyzed by gel electrophoresis (3% agarose).

Plastic Sections

Larvae and adult eyes were fixed at least overnight in 4% formaldehyde at 4°C and embedded in Technovit 7100 (Kulzer, Wehrheim, Germany). Samples were sectioned at 3 µm thickness on a microtome (LeicaRM2145, Leica Microsystems, Nussloch, Germany) and sections were stained in Richardson solution (1% methylene blue, 1% borax) for 20 seconds, washed for 10 minutes in ddH_2O and coverslipped with Entellan mounting medium (Merck, Darmstadt, Germany). Images were acquired on an Olympus BX61 microscope and analyzed using Fiji ImageJ (National Institutes of Health, Bethesda, MD, USA). Statistical analysis of eye size or retinal layers was carried out using mixed-repeated measures ANOVA and Tukey and Games-Howell post hoc tests.

Immunohistochemistry

Larvae and adult eyes were fixed for 2 hours in 4% formaldehyde at 4°C, cryo-protected in 30 % sucrose overnight at 4°C, embedded in Richard-Allan Scientific Neg-50 Frozen Section Medium (Thermo Fisher Scientific, Kalamazoo, MI, USA) and cryo-sectioned at 16-µm thickness. Primary antibodies were rabbit anti-Cacna1fa (1:6000, kindly provided by Michael Taylor, School of Pharmacy, University of Wisconsin-Madison), rabbit anti-RibeyeA (1:2500), rabbit anti-RibeyeB (1:250, both Ribeye antibodies kindly provided by Teresa Nicholson, Oregon Health & Science University), rabbit anti-mGluR6b (1:750)[36] and mouse anti-Zpr-1 (1:400; Zebrafish International Resource Center, Eugene, OR, USA). Secondary antibodies were goat anti-rabbit and anti-mouse IgG conjugated to Alexa 488, 568, or 647 (1:500 to 1:1000, Molecular Probes, Life Technologies, Eugene, OR, USA). Sections were coverslipped with Mowiol (Polysciences, Warrington, PA, USA) containing DABCO (Sigma-Aldrich, Steinheim, Germany) and

Investigative Ophthalmology & Visual Science

Downloaded from iovs.arvojournals.org on 12/16/2019

imaged with a TCS LSI confocal microscope (Leica Microsystems). All microscopy images were analyzed and adjusted for brightness and contrast using ImageJ.

CLEM and TEM

Correlative light and electron microscopy (CLEM) was carried out as described.[37,38] Briefly, 5 dpf larvae were euthanized in tricaine (ethyl 3-aminobenzoate methanesulfonate, Sigma-Aldrich) and fixed in a mixture of 0.1 M sodium cacodylate buffer, 4 % formaldehyde and 0.025% glutaraldehyde over night at 4°C. Subsequently eyes were dissected and one eye per larva washed in 1X PBS, placed in warm 12 % gelatin for 10 minutes at 40°C and finally left to harden at 4°C. Embedded eyes were immersed in 2.3 M sucrose and stored at 4°C for CLEM. The second eye was used for TEM and was transferred to a mixture of 2.5% glutaraldehyde and 0.1 M sodium cacodylate buffer and kept overnight at 4°C. Subsequently the sample was washed with fresh 0.1 M sodium cacodylate buffer and stored at 4°C.

TEM samples were incubated in 1% osmium tetroxide in 0.1 M cacodylate buffer for 1 hour on ice. After rinsing, samples were treated with UAc 1% in water for 1 hour at room temperature (RT), subsequently dehydrated in an ethanol series and embedded in Epon. Seventy nm sections were post stained with Reynold's lead solution for 5 minutes and examined with a transmission electron microscope (Talos 120, Thermo Fisher Scientific) equipped with MAPS, a modular software application for automated acquisition of high resolution images from large areas. One section per individual ($n = 3$ per genotype) was scanned on the level of photoreceptor synapses along the length of the retina. Statistical analysis of synapse and synaptic ribbon number was carried out using repeated-measures ANOVA with Bonferroni correction or odds ratio using a general linear model.

CLEM samples were frozen in liquid nitrogen and sectioned with a cryo-ultramicrotome (Ultracut EM FC6, Leica Microsystems) using a cryo immuno diamond knife (Diatome). 110 nm ultrathin sections were transferred to a 7 × 7-mm silicon wafer (Si-Mat Silicon Materials, Kaufering, Germany) and stored at 4°C. Rabbit anti-Cacna1fa (see section Immunohistochemistry) was used 1:500 in PBG (PBS with 0.5% Bovine serum albumin and 0.2% gelatin type B) and wafers were incubated 50 minutes at RT. Secondary goat anti-rabbit (AF568 F(ab')2, Life tech A21069, Lot 1387794) was used at 1:200 in PBG for 30 minutes at RT. After light microscopy imaging the wafers were fixed with 0.1% glutaraldehyde, incubated with methylcellulose followed by centrifugation and imaged with a scanning electron microscope (Auriga 40, CrossBeam; Carl Zeiss Microscopy, Jena, Germany) at low voltage (1.5 keV).

ERG

White-light ERG measurements were carried out as described,[39] with adaptations.[40] We dark adapted 5 dpf and 20 dpf KO lines and controls for 30 minutes prior to stimulation. Five 100-ms flashes of increasing light intensity (ranging from log-4 to log0, where log0 corresponds to 24,000 $\mu W/cm^2$) were applied with an inter-stimulus interval of 7000 ms. For the flicker fusion ERG, flickering stimuli of 2012 $\mu W/cm^2$ were displayed at frequencies from 1 to 26 Hz (at 10% duty cycle) with background irradiance of 24 $\mu W/cm^2$. Statistical analysis of b-wave amplitudes were carried out using mixed repeated-measures ANOVA followed by Tukey and Games-Howell post hoc test and Bonferroni-corrected pairwise comparisons (WT vs. single-KO) or independent samples *t*-test for each light intensity or the flicker fusion threshold, respectively (WT vs. double-KO).

Results

Identification and Expression Analysis of Two *CACNA2D4* Homologues in Zebrafish

We identified two zebrafish orthologs of human *CACNA2D4,* named *cacna2d4a* and *cacna2d4b*, by searching the zebrafish genome database against verified human and mouse sequences of $\alpha_2\delta$ subunit family members as well as phylogenetic analysis of the totally eight identified zebrafish genes of the *Cacna2d* family (Fig. 1A). Both paralogs contain the predicted functional domains, namely the Von Willebrand Factor A (VWA) and VWA N-terminal domain,[41] a Cache domain,[42] and an ω site required for GPI-anchoring (Fig. 1B). Both paralogues are expressed in the retina, with slight differences in expression pattern during development (Fig. 1C). In 3 days post fertilization (dpf) zebrafish, *cacna2d4a* mRNA is detected predominantly in the inner nuclear layer (INL), harboring bipolar, horizontal, and amacrine cells, besides a faint signal in the peripheral outer nuclear layer (ONL). Apart from a strong signal in the ONL, *cacna2d4b* mRNA was found in the INL and in the cerebellum. We did not detect any staining outside of the retina besides this cerebellar expression. The partially divergent expression patterns in larvae become more similar in the adult zebrafish retina, where the mRNA of both paralogs is detected in the ONL and INL.

$\alpha_2\delta_4$-KO Impairs $Ca_v1.4$ Expression and Localization and Affects Retinal Function

We created CRISPR/Cas9 knock out (KO) lines for *cacna2d4a* and *cacna2d4b* by targeting exon 4 of *cacna2d4a* and exon 8 of *cacna2d4b*, respectively. We selected lines with frameshift mutations predicting a premature stop codon and consequently a truncated protein in mutants (*cacna2d4a*-KO and *cacna2d4b*-KO; Supplementary Figs. S1). Since $\alpha_2\delta$ subunits are known to set the abundance of Ca_v1 channels (reviewed in Ref. 21), we hypothesized that $\alpha_2\delta_4$ takes up a similar role at the photoreceptor ribbon synapse. We therefore investigated the localization of Cacna1fa, the pore-forming subunit of $Ca_v1.4$ in photoreceptors of zebrafish,[20] in wild type and KO animals at different developmental stages (Figs. 2A, 2B). KO of *cacna2d4a* did not lead to changes in expression of Cacna1fa at 5 dpf; however, lack of *cacna2d4b* not only reduced the abundance of Cacna1fa at the photoreceptor terminals, but also led to the appearance of Cacna1fa puncta more distal of the plexiform layer (arrows). This phenotype was also found in older larvae (20 dpf).

In *cacna1fa*-KO fish, ERG responses are completely absent.[20] We therefore tested whether the decrease in Cacna1fa expressed at the synapse of *cacna2d4b*-KO fish leads to impaired signal transmission. To this end, we performed ERG measurements on dark-adapted wild type, *cacna2d4a*-KO, and *cacna2d4b*-KO larvae at 5 dpf, with five white light flashes of increasing light intensity. As expected from Cacna1fa immunohistochemistry, b-wave amplitudes of wild type and *cacna2d4a*-KO larvae were comparable. However, surprisingly, also b-wave amplitudes of *cacna2d4b*-KO were normal (Fig. 3A).

To test whether the discrepancy between Cacna1fa expression and retinal function in *cacna2d4b*-KO larvae was due to compensation by Cacna2d4a, we crossed *cacna2d4a*-KO with *cacna2d4b*-KO lines to create a double-KO line. Cacna1fa expression in double-KO is comparable to the

Investigative Ophthalmology & Visual Science

Downloaded from iovs.arvojournals.org on 12/16/2019

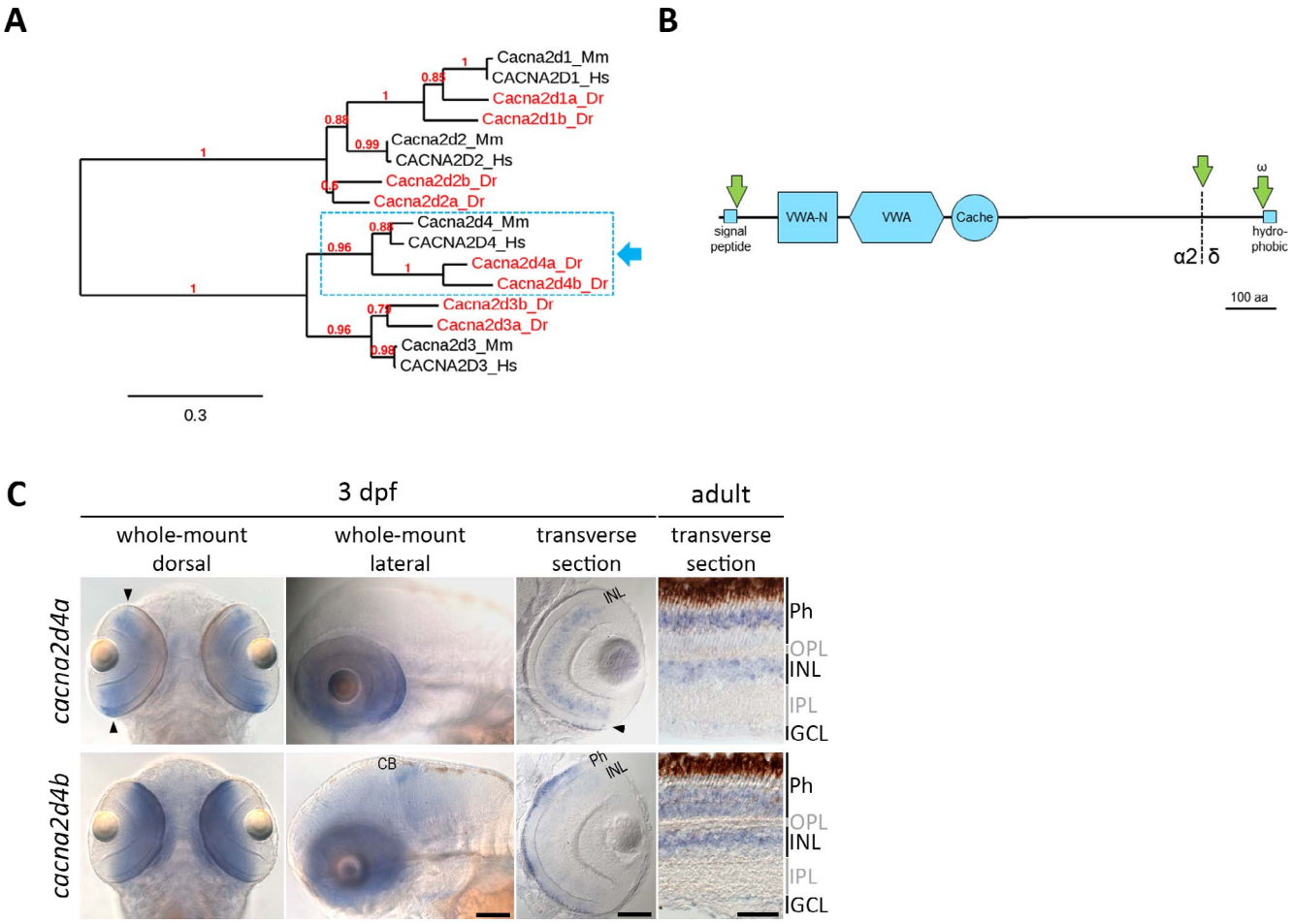

Figure 1. Bioinformatic and expression analysis of the zebrafish orthologues of Cacna2d4. (**A**) Maximum likelihood phylogenetic tree of the Cacna2d family. Eight members were identified in the zebrafish genome, two of which are clear orthologues of mammalian Cacna2d4 (*dashed box*). (**B**) Schematic representation of predicted protein structure applying to both members of the Cacna2d4 subclade (*dashed box* in **A**). Cacna2d4 proteins contain Van-Willebrand factor (VWA) and VWA N-terminal (VWA-N) domains, as well as one Cache domain, an N-terminal signal peptide and a ω site adjacent to a short C-terminal hydrophobic region, predicted to mediate proteolytic cleavage and GPI anchoring. Proteolytic cleavage (*dashed line*) of the Cacna2d4 pro-form gives rise to α2 and δ peptides, which remain attached to each other through disulfide bonds in mature α2δ proteins. (**C**) In situ hybridization of zebrafish *cacna2d4a* and *cacna2d4b*. In 3 dpf zebrafish, *cacna2d4a* is expressed throughout the retinal INL and in photoreceptors (Phs) of the retinal periphery (*arrowheads*). In the adult retina, *cacna2d4a* is expressed in the INL and the distal half of the Ph layer. In larval zebrafish, *cacna2d4b* shows strong expression in Phs, weak expression in the INL and additional signal in the cerebellum. In the adult retina, *cacna2d4b* is expressed across the Ph layer and in the INL. *Arrows* in (**B**) indicate proteolytic cleavage. aa, amino acids; CB, cerebellum; Dr, Danio rerio; GCL, ganglion cell layer; Hs, Homo sapiens; Mm, Mus musculus. *Scale bars* correspond to 100 μm in images of 3 dpf zebrafish and 50 μm in adult sections.

findings in *cacna2d4b*-KO larvae (Fig. 2A), while in adult retinae it appears to reach wild type levels (Fig. 2B). Nonetheless, there are still puncta ectopic to the OPL. Despite having a similar abundance of Cacna1fa as *cacna2d4b*-KO larvae, double-KO at 5 dpf exhibited a significantly decreased b-wave amplitude from dim to bright light stimuli (Figs. 3B, 3D) and slower b-wave kinetics (Fig. 3C), both indicative of impaired signal transmission. Since measurements were taken at a developmental stage (5 dpf) where the visual system of the zebrafish is exclusively cone-driven,[43,44] we conclude that cone synaptic transmission is impaired, but not absent in double-KO zebrafish at 5 dpf.

To test whether photoreceptor function deteriorates or recovers over time, we measured the ERG responses at 20 dpf, when the retina is more mature and also rods contribute to the light response. When measuring the white light ERG under the same conditions as at 5 dpf, we recorded mixed rod-cone responses that were not attenuated in amplitude (Fig. 4A). Surprisingly, at dim to medium light (log-3), the responses of double-KOs were even slightly stronger than in wild types. Nevertheless, response kinetics in double-KO fish were slower compared to wild type at almost all light intensities (Fig. 4B). This resembled the findings in 5 dpf larvae, where cone responses were delayed. To test whether the slower kinetics affect temporal resolution of cones we measured the flicker fusion threshold of 20 dpf wild type and double-KO. For this, we displayed flickering stimuli of 2012 μW/cm^2 irradiance from 1 to up to 26 Hz under photopic conditions (background irradiance of 24 μW/cm^2—an irradiance of 5 μW/cm^2 is regarded as sufficient to saturate rods in fish[45]). The stimulus frequency at which the response does not resolve the individual stimuli anymore and becomes steady is termed the flicker fusion threshold. We found that the flicker fusion threshold [Hz] was significantly lower in double-KO compared to wild type at 20 dpf, indicating that also in the more mature retina cone function is disturbed (Fig. 4C).

With these results we confirm that targeting of the α_1 subunit of $Ca_v1.4$ to the synaptic membrane is an evolution-

Investigative Ophthalmology & Visual Science

Downloaded from iovs.arvojournals.org on 12/16/2019

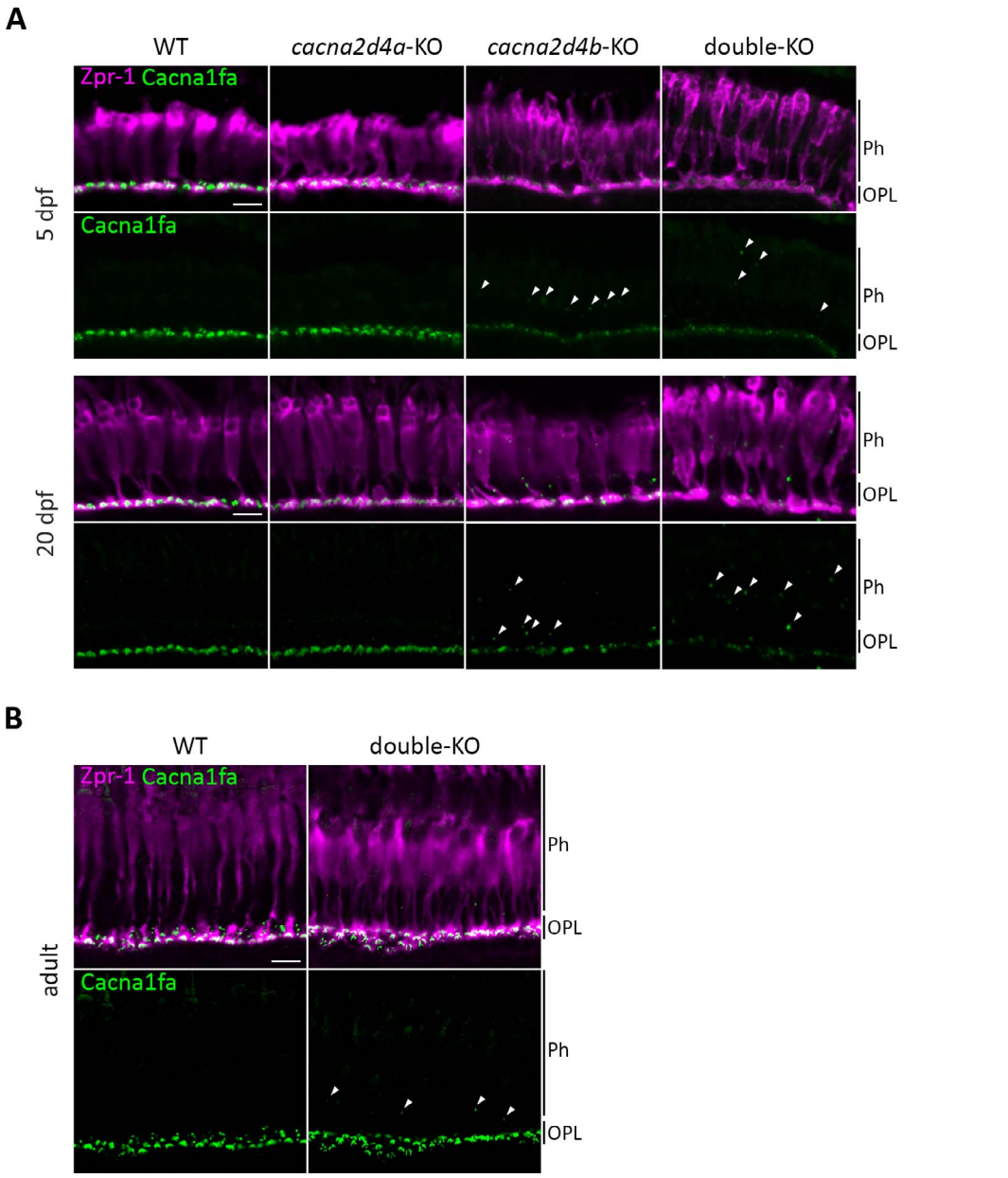

Figure 2. Cacna1fa localization *cacna2d4*-KO lines. (**A**) Immunohistochemical analysis of Cacna1fa with Zpr-1 counterstain (*red-green double cones*). Cacna1fa expression is not affected in *cacna2d4a*-KO larvae at 5 and 20 dpf, but severely reduced in *cacna2d4b*-KO as well as in double-KO. In the latter two, ectopic punctate Cacna1fa staining is observed distal to the OPL (*arrowheads*). (**B**) Expression in adult double-KO is comparable to WT levels, yet ectopic puncta are visible (*arrowheads*). *Scale bars* (**A**, **B**) correspond to 10 µm and apply to all images of the respective developmental stage.

arily conserved function of Cacna2d4. We also show that the density changes in Cacna1fa expression alone are not sufficient to induce impaired signal transmission. In addition, we found that cone dysfunction persists beyond 5 dpf in double-KO.

Loss of $\alpha_2\delta_4$ Leads to Minor Changes in Retinal Morphology

To investigate whether mutations in *cacna2d4a* and/or *cacna2d4b* affect overall retinal development and morphology, and whether such phenotypes are progressive, we analyzed semi-thin plastic sections of *cacna2d4*-KO, *cacna2d4b*-KO and double-KO zebrafish at 5 dpf, 20dpf and adulthood (Fig. 5). Of particular interest was the outer plexiform layer (OPL), the most affected retinal layer in *cacna1fa*-KO zebrafish[20] and *cacna2d4* mutant mice.[6,23,24]

Loss of any of the $\alpha_2\delta_4$ subunits leads to decreased eye size at 5 dpf (Fig. 5B). In addition, double-KO larvae showed reduced central retinal thickness at this stage (Fig. 5C). Since the ONL as well as the OPL were not decreased relative to total central retinal thickness in any of the mutants at any developmental stage (Figs. 5D, 5E), we conclude that, in accordance with the non-degenerative phenotype in patients,[22,46] the smaller eye size is neither due to photoreceptor degeneration nor the result of malformation of the OPL. This was further supported by TUNEL and PCNA (proliferating cell nuclear antigen) staining, where we did not observe changes in apoptotic or proliferating cells, respectively, in the central

Investigative Ophthalmology & Visual Science

Downloaded from iovs.arvojournals.org on 12/16/2019

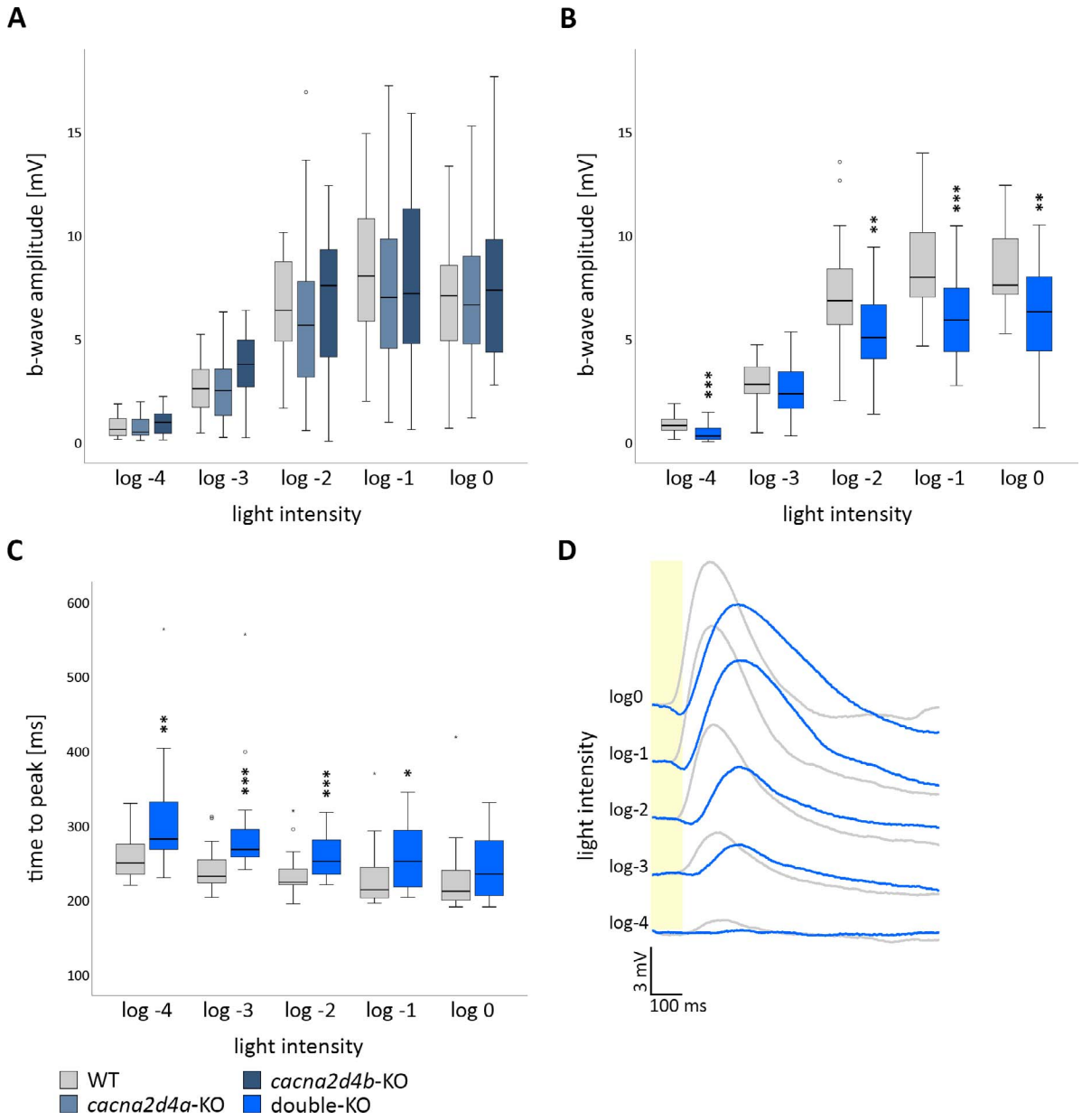

Figure 3. Retinal function of *cacna2d4*-KO lines at 5 dpf. (**A–C**) *Box* and *whisker* plots of white-light ERG b-wave amplitudes or b-wave kinetics of 5 dpf WT, *cacna2d4a*-KO, *cacna2d4b*-KO and double-KO. *Bottom and top of the box*, the first and third quartile; median, *line within the box*; *whiskers*, minimum and maximum values; *circles*, outliers (1.5 × interquartile distance); *small asterisks*, extreme outliers (3 × interquartile distance). Five flashes (100 ms) of increasing light intensities were applied, starting from dim light (log-4) to 100% light intensity (log0, 24,000 µW/cm), and responses were grouped accordingly. (**A**) Neither *cacna2d4a* nor *cacna2d4b*-KO disturbed the ERG response at any light intensity ($n = 27$ per genotype). (**B**) KO of both paralogs significantly reduced the b-wave amplitude at different light intensities ($n = 25$ per genotype). (**C**) The time from baseline to peak is significantly prolonged in double-KO retinae. Significance levels: $^{*}P \leq 0.05$, $^{**}P \leq 0.01$, $^{***}P \leq 0.001$. (**D**) Example traces of WT (*gray*) and double-KO (*blue*). *Yellow bar* in (**D**) represents the stimulus.

retina (data not shown). This also suggests that the retinal dysfunction in double-KO larvae occurs independently of gross morphological changes in the OPL. At 20 dpf eye size of double-KO was still significantly smaller compared to wild type (Fig. 5B), however, central retinal thickness appeared normal (Fig. 5C), indicating normal development but potentially slower proliferation in the periphery. Although we did not observe obvious differences in the PCNA labeling in the peripheral retina, we cannot exclude the possibility for more subtle changes in proliferation, undetectable by the used methods.

In the adult retina, we did not find any significant changes in retinal layering in any of the KO lines (Figs. 5A, C–E). In summary, neither *cacna2d4a* nor *cacna2d4b* are essential for maintenance of correct retinal morphology, and the visual defect in double-KO does not lead to retinal degeneration. Instead, loss of both paralogs may lead to developmental delay.

Impact of $\alpha_2\delta_4$ on Ribbon Synapse Structure and Localization

Zebrafish lacking Cacna1fa show a severe reduction in Ribeyeb expression in the OPL. Hence, it was suggested that Cacna1fa

Investigative Ophthalmology & Visual Science

Downloaded from iovs.arvojournals.org on 12/16/2019

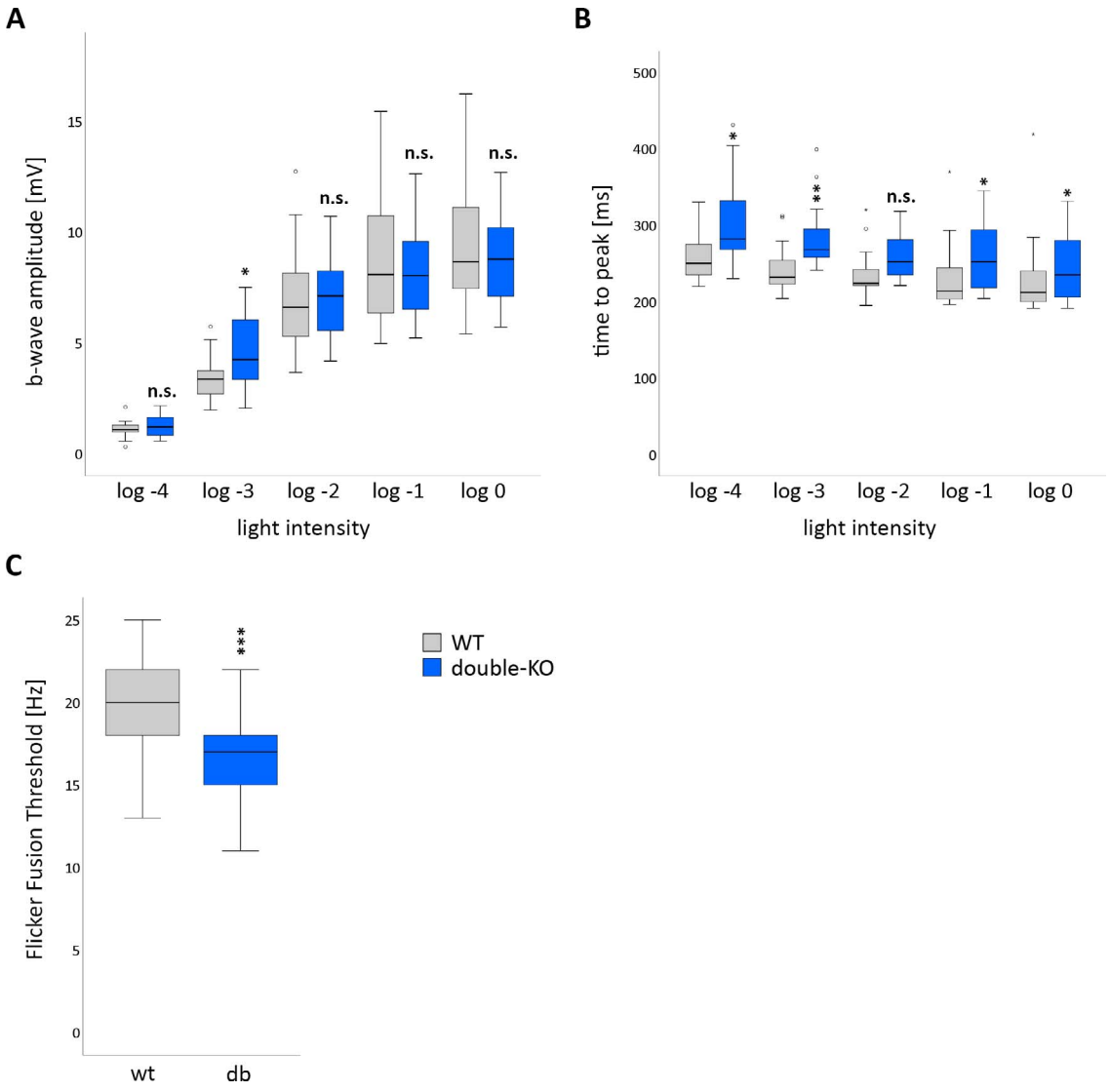

FIGURE 4. Retinal function of *cacna2d4*-KO lines at 20 dpf. (**A**–**C**) *Box and whisker* plots of white-light ERG b-wave amplitudes, b-wave kinetics and flicker fusion threshold of 20 dpf WT and double-KO. *Bottom and top of the box*: the first and third quartile; *median*, line within the box; *whiskers*, minimum and maximum values; *circles*, outliers (1.5 × interquartile distance); *small asterisks*, extreme outliers (3 × interquartile distance). (**A**, **B**) Five flashes (100 ms) of increasing light intensities were applied, starting from dim light (log-4) to 100% light intensity (log0, 24,000 µW/cm2), and responses were grouped accordingly ($n = 19$ per genotype). (**A**) b-wave amplitude of the mixed rod-cone response was not attenuated in double-KO. (**B**) The time from baseline to peak is significantly prolonged in double-KO at almost all light intensities. (**C**) The flicker fusion threshold is reduced in double-KO under photopic conditions ($n = 25$ per genotype). Significance levels: $^{*}P \leq 0.05$, $^{**}P \leq 0.01$, $^{***}P \leq 0.001$.

is essential for the development of synaptic ribbons.[20] Since Ribeyeb is the main structural component of the synaptic ribbon in zebrafish photoreceptors,[47] we tested whether Ribeyeb expression was affected upon KO of *cacna2d4b* and the concomitant lower synaptic Cacna1fa levels. Surprisingly, *cacna2d4b*-KO as well as double-KO larvae (at 5 and 20 dpf) showed normal Ribeyeb expression levels (Fig. 6A). This suggests that presence of Cacna2d4 is not essential for Ribeyeb expression and that a mere reduction in Cacna1fa levels is not sufficient to destabilize Ribeyeb. It was therefore not surprising to find that Ribeyeb expression in the double-KO adult retina was similar to control (Fig. 6A), since also Cacna1fa expression seems to be normalized at this stage (Fig. 2B).

Most interestingly, we observed ectopic Ribeyeb staining in both *cacna2d4b*-KO and double-KO retinae (Fig. 6A, arrows). This is reminiscent of mislocalized Cacna1fa puncta in these lines (Fig. 2) and resembles the phenotype found in *cacna1fa*-KO zebrafish, where Ribeyeb, present at only very low levels, is mislocalized towards the inner segment.[20] In addition, mice with synaptopathies, including *Cacna2d4*-KO mice, show outgrowth of horizontal cell and bipolar cell synapses into the ONL, where they form ectopic synapses with photoreceptors.[4,17,23,24,48–50] Therefore, the ectopic punctate Cacna1fa and Ribeyeb expression might reflect the presynaptic portion of such ectopically formed synapses. On the postsynaptic side, however, we did not detect changes in mGluR6b localization (Fig. 6B). This implies that the remaining channels are sufficient to preserve the apposition of pre- and postsynapse and that mGluR6b is not part of the putative ectopic synapses.

To verify that the remaining α_1F subunits in double-KO are correctly localized within the synaptic layer, we performed correlative light- and electron microscopy (CLEM). Staining with Cacna1fa antibody yielded fewer puncta in the OPL of double-KO (Fig. 7A), consistent with the low expression found by

Investigative Ophthalmology & Visual Science

Downloaded from iovs.arvojournals.org on 12/16/2019

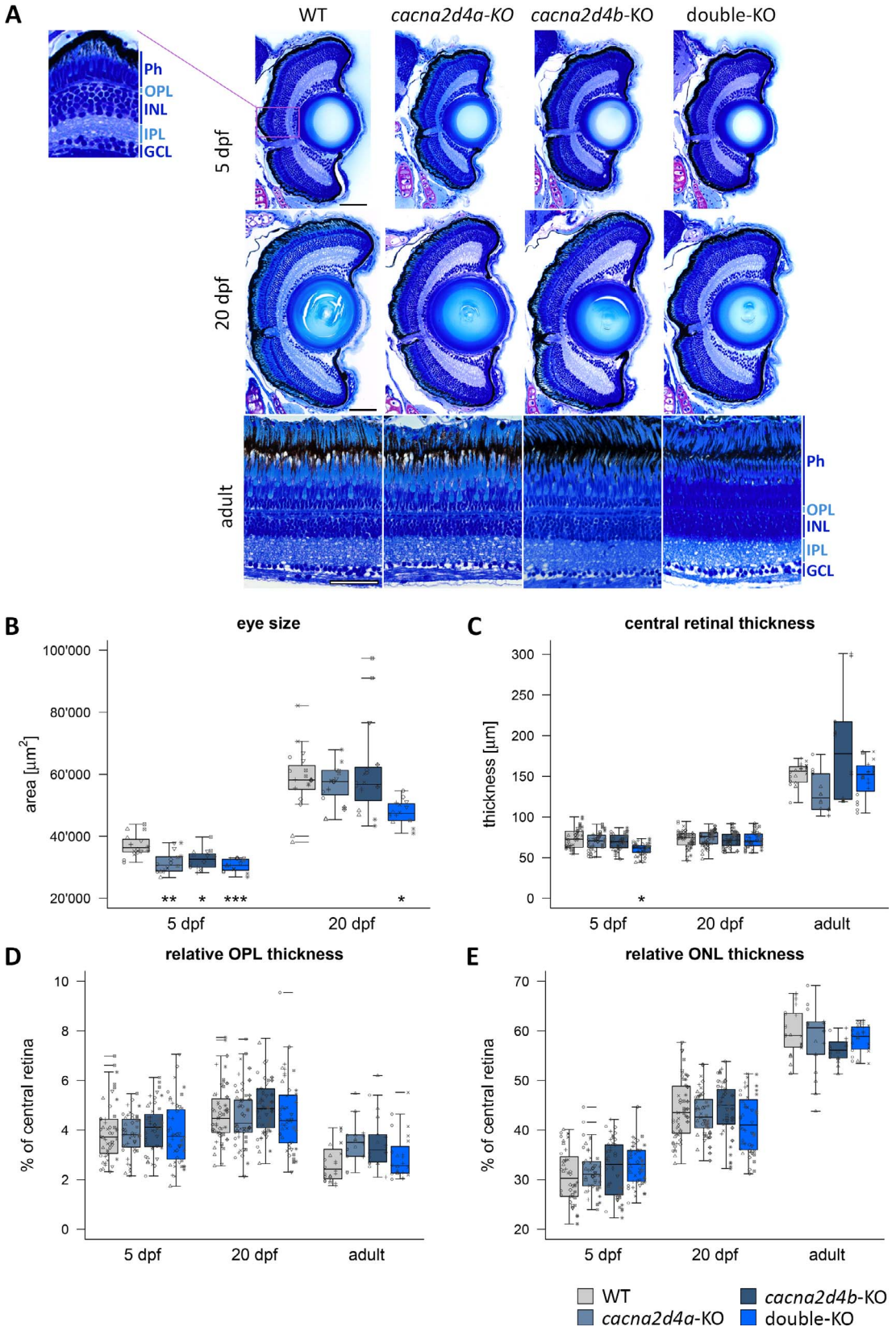

Figure 5. Morphologic analysis of *cacna2d4*-KO retinae. (**A**) Semithin plastic sections (3 µm) of WT, *cacna2d4a*-KO, *cacna2d4b*-KO and double KO retinae at 5 dpf, 20 dpf, and adult (>5 months). (**B–E**) Quantification of eye size and retinal layers. Three measurements per section were taken from the central retina, close to the optic nerve. For 5 and 20 dpf fish, eye circumference on central sections was measured as an approximation for eye size. In larvae, both eyes were analyzed, yielding two data points for eye size and six for retinal layers per fish. In adult retinas, two sections per retina and three measurements per section were taken from the central retina, adding to a total of six measurements per fish. 5 dpf: $n = 8$ each, 20 dpf: WT $n = 10$; *cacna2d4a*-KO $n = 10$; *cacna2d4b*-KO $n = 10$; double-KO $n = 8$, adult: WT $n = 4$, *cacna2d4a*-KO $n = 3$, *cacna2d4b*-KO $n = 3$,

Investigative Ophthalmology & Visual Science

Downloaded from iovs.arvojournals.org on 12/16/2019

double-KO $n = 4$). Box and whisker plots: *bottom and top of the box* = first and third quartile; the median = *line within the box*; whiskers = minimum and maximum values; data points with the same shape correspond to the same animal in each box; horizontal lines = outliers. Significance levels: $^{*}P \leq 0.05$, $^{**}P \leq 0.01$, $^{***}P \leq 0.001$. *Scale bars* in (**A**) correspond to 50 µm and apply to all images of the respective developmental stage.

regular immunohistochemistry. Correlation of the antibody staining with the EM image revealed that not only in WT Cacna1fa localizes to the base of synaptic ribbons, but that this is also true for double-KO (Fig. 7A, close up). To the best of our knowledge, we here demonstrate for the first time directly that a Cacna1f homolog localizes to the plasma membrane compartment directly opposing the base of a synaptic ribbon, and that its localization is highly confined to this membrane domain.

Finally, we tested the integrity and localization of synaptic ribbons on the ultrastructural level by transmission electron microscopy (TEM; Fig. 7B–E). We found that double-KO retinae harbor a normal number of synapses at 5 dpf, but the number of ribbons is reduced compared to control (Fig. 7C). Furthermore, 'floating' ribbons (not attached to the active zone) were more abundant in double-KO (Fig. 7C), also relative to the total number of ribbons (Fig. 7E). Interestingly, we found more synapses without ribbons in double-KO while at the same time we found less synapses harboring more than one ribbon (cones), but equal numbers of synapses with only one ribbon (mostly rods; Fig. 7D). Therefore, the formation and/or maintenance of ribbons in a subset of synapses, most probably representing cones, is impaired upon KO of both paralogs, while rod synapses seem less affected.

Discussion

In this study we identified two zebrafish orthologs of human *CACNA2D4*, harboring the canonical protein domain composition typical of all $\alpha_2\delta$ family members, indicative of functional conservation. We found that Cacna2d4b is essential for synaptic expression of Cacna1fa in photoreceptors of larval zebrafish, comparable to mouse Cacna2d4[23,24] and other $\alpha_2\delta$ subunits.[51–53] In zebrafish, the two paralogs show partial subfunctionalization: *cacna2d4a*-KO did not affect Cacna1fa expression, which is consistent with its more prominent expression in the INL. Nevertheless, either subunit is sufficient to maintain wild type levels of signal transmission and only the combined loss of both paralogs affected ERG b-wave amplitude and its kinetics at 5 dpf. The slower kinetics of the ERG response was still apparent in the more mature retina of double-KO at 20 dpf and led to a decrease in temporal resolution under photopic conditions. The differences between single- and double-KO support the notion that Cacna2d4a impacts cone signal transmission through a function apart from $Ca_v1.4$ forward trafficking. The expression of *cacna2d4a* in the INL is unlikely to account for the impaired b-wave via direct modulation of Cacna1fa activity at the photoreceptor synapse. However, *cacna2d4a* expression in the peripheral photoreceptor layer might point to a transient role in photoreceptor development. Loss of *cacna2d4a* could therefore indirectly affect signal transmission at the ribbon synapse. The impaired anchoring and partial loss of ribbons in synapses of double-KO retinae supports the notion that $\alpha_2\delta_4$ subunits are involved in development/maintenance of synaptic ribbons.

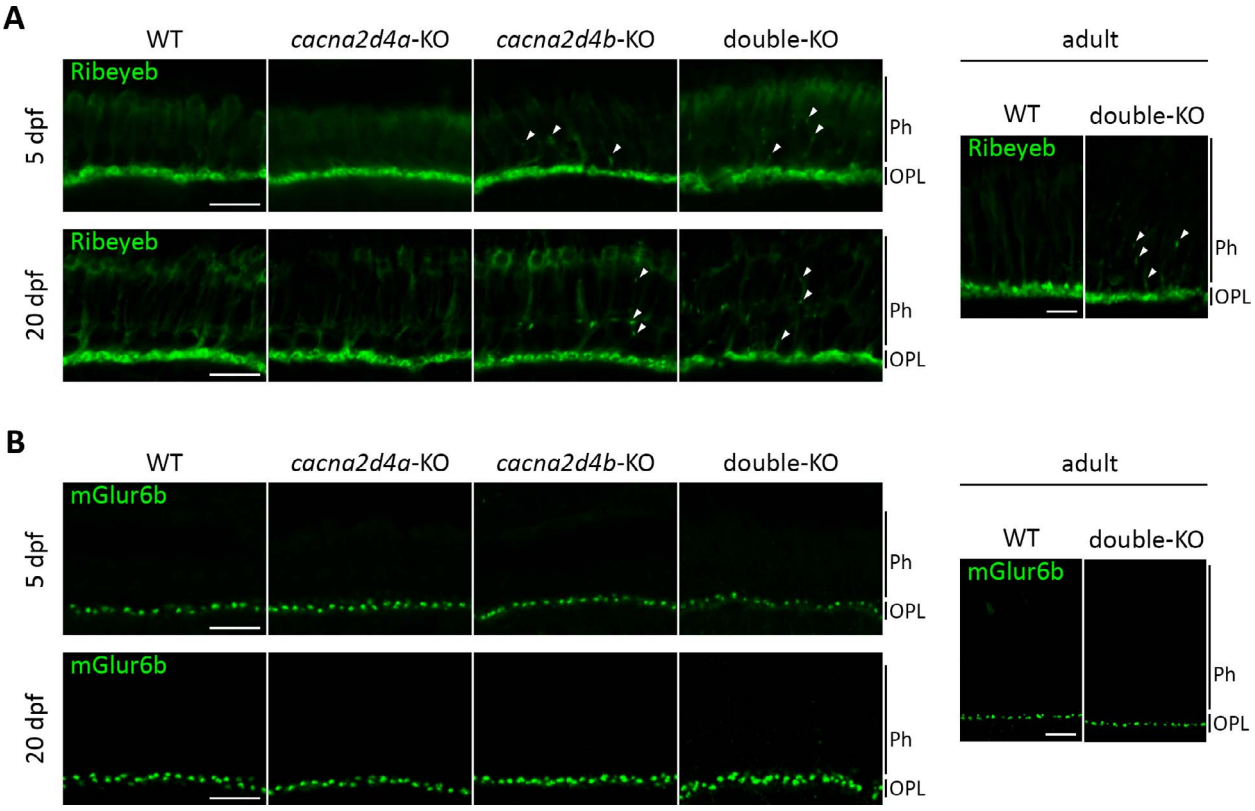

Figure 6. Ribeyeb expression in *cacna2d4*-KO lines. (**A**) Ribeyeb expression levels in the OPL of 5 dpf, 20 dpf and adult retina are not affected by mutations in *cacna2d4* genes. However, both *cacna2d4b*-KO and double-KO show ectopic Ribeyeb staining distal to the OPL at all ages examined. (**B**) mGluR6b expression is comparable to WT in all KO lines.

Investigative Ophthalmology & Visual Science

Downloaded from iovs.arvojournals.org on 12/16/2019

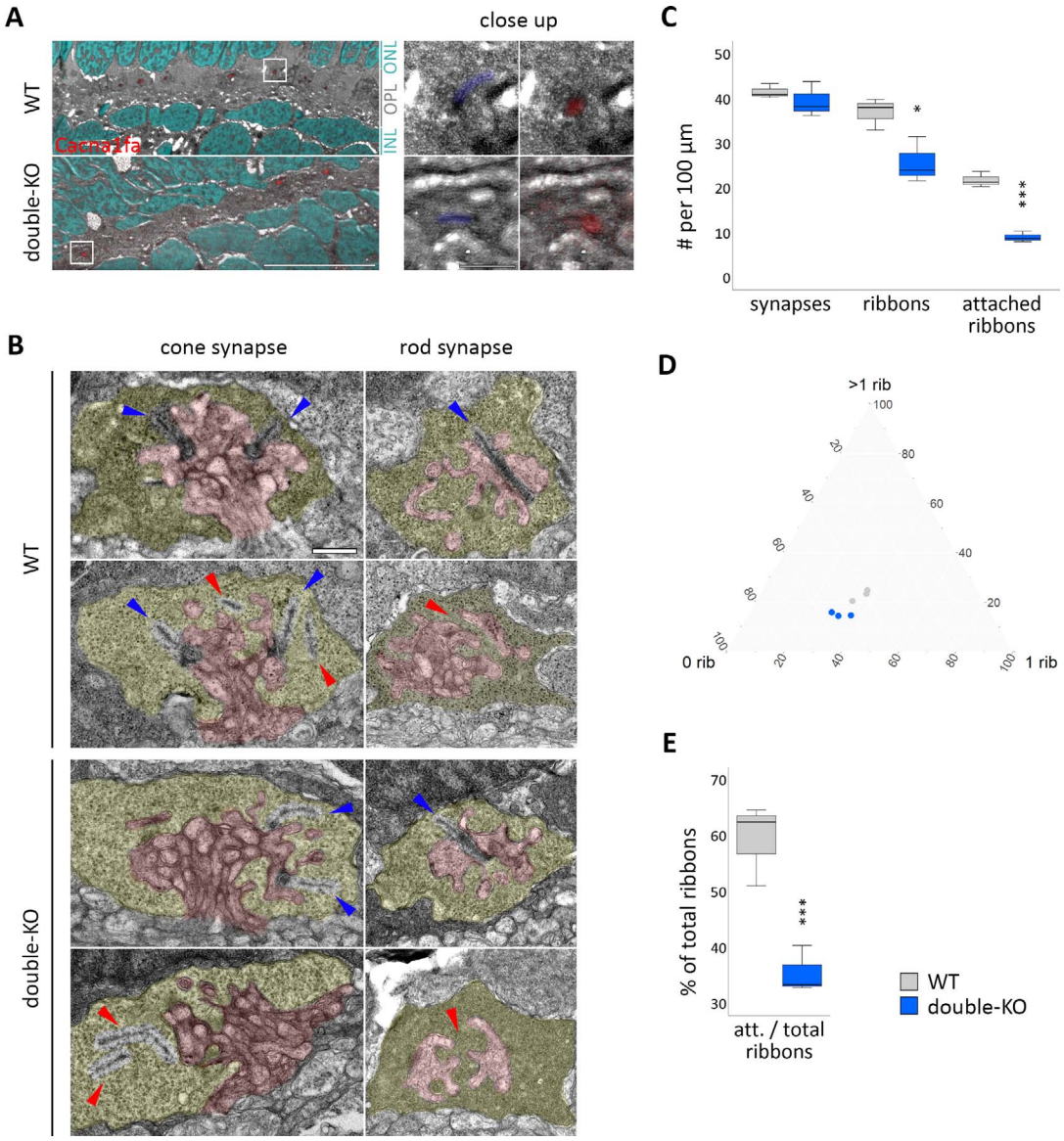

Figure 7. Ultrastructure of the photoreceptor ribbon synapse. (**A**) Correlative light- and electron microscopy (CLEM) on 5 dpf retinae of WT and double-KO. Cacna1fa puncta seem to be reduced in number in double-KO compared to WT, but both show correct localization of Cacna1fa to synaptic ribbons in the OPL (close up). *Red*: Cacna1fa antibody staining. *Cyan*: DAPI. *Blue*: pseudo-colored ribbon. *White frame*: close up region. *Scale bar* in overview corresponds to 10 µm and in close-up to 1 µm. (**B**) Transmission electron micrographs (TEM) of synapses in 5 dpf WT and double-KO. The presynaptic terminal is pseudocolored in *yellow* and the postsynaptic invaginations in *red*. Ribbons that are attached to the active zone are found in cones and rods of both genotypes (*blue arrows*), but also some that are 'floating' or missing (*red arrows*). *Scale bar*: 0.5 µm. (**C–E**) Quantification of synapse and ribbon number or attachment on whole-retinal scans of three sections per genotype (one per individual). (**C**) The number of synapses per 100 µm in double-KO is normal, however the amount of ribbons is reduced and there are fewer ribbons attached to the active zone. (**D**) Ternary plot of synapse subtypes: 0 rib = empty synapses; 1 rib = synapses with one ribbon; >1 rib = synapses with more than one ribbon; grey = WT; blue = double-KO. The data from WT and double-KO form two separate clusters. The percentage of synapses harboring more than one ribbon (cones) is lower ($P = 0.03$) and that of empty synapses is higher ($P = 0.05$) in double-KO. 1-ribbon synapses do not seem to be affected. (**E**) The number of attached ribbons relative to the total number of ribbons is lower in double-KO retinae. *Box and whisker plots*: *bottom and top of the box*, first and third quartile; the *median*, line within the box; *whiskers*, minimum and maximum values. Significance levels: $^{*}P \leq 0.05$, $^{**}P \leq 0.01$, $^{***}P \leq 0.001$.

Interestingly, even though we found the cone ERG responses to be significantly impaired, the amplitude of the b-wave was only slightly reduced, which is in accordance with the rather mild ERG defect in patients,[7,22,46] but in contrast to the more severe phenotype in *cacna2d4*-KO mice.[6,23,24] Furthermore, we were surprised to find that loss of Cacna2d4a and b together with the substantial reduction in Cacna1fa levels did not elicit a stronger effect on ERG response as well as on ribbon synapse structure and general retinal morphology in double-KO. This is particularly surprising in light of the strong defects in *cacna1fa*-KO zebrafish and the fact that not only Cacna1fa was proven important for ribbon synapse development and maintenance in zebrafish,[20] but also Cacna2d4 was shown to have a similar function in murine rod photoreceptors.[23,24] The remaining channels are very likely still functional, supported by residual Cacna1fa labeling that we find to be associated with synaptic ribbons. In addition, calcium influx dependent Ribeyeb expression in cones[20] is unaffected. Both

Investigative Ophthalmology & Visual Science

Downloaded from iovs.arvojournals.org on 12/16/2019

findings point towards the possibility that in double-KO photoreceptors adequate Ca^{2+}-currents are produced to maintain synaptic transmission, albeit at lower levels. Furthermore, other Ca_v and modulation by other $\alpha_2\delta$ subunits may also contribute to synaptic transmission.[16,54]

Since *cacna2d4a* and *cacna2d4b* are both expressed in photoreceptors in adults, it was interesting to see that in the absence of both paralogs the phenotype did not worsen compared to larvae, but rather improved by restoring Cacna1fa expression to wild type levels. We therefore propose that $\alpha_2\delta_4$ in zebrafish is most important during development. Potentially at later stages, other subunits such as β_2[5,55] take over forward trafficking of Cacna1fa. The only difference to adult wild type was that we still found ectopic punctate expression of Cacna1fa as well as Ribeyeb, possibly representing ectopically forming synapses.

Finally, based on the findings above, it is not surprising that the relatively mild retinal dysfunction did not affect retinal morphology and did not cause any degeneration of photoreceptors. Interestingly, our data is consistent with a delay of development as judged by eye size at 5 dpf. At this prefeeding stage, this delay cannot be explained by poorer prey catching performance. Therefore, $\alpha_2\delta_4$ may have an unknown function during development that is independent from its better understood function in the mature retina.

Taken together, we present in this study a new zebrafish model to study human diseases related to *CACNA2D4*-dysfunction. Despite harboring two orthologs of human *CACNA2D4* that have slightly divergent expression and function in the zebrafish retina, KO of both paralogs effectively mimicked the mildly impaired cone visual function of patients and the slowly or nondegenerative nature of the defect. The divergent expression of Cacna2d4 in larvae can be exploited to investigate the completely unstudied role of $\alpha_2\delta_4$ in bipolar cells. Finally, the ectopic expression of Cacna1fa in our model provides an opportunity to study Ca^{2+}-channel trafficking to presynaptic sites.

Acknowledgments

The authors thank Reinhard Furrer for expert statistical advice, Teresa Nicholson and Michael Taylor for providing Ribeye and Cacna1fa antibodies, Christian Mosimann and Martin Jínek for the Cas9-GFP fusion protein, and Martin Walther and Kara Kristiansen for fish care and technical support.

Supported by Robert und Rosa Pulfer-Stiftung, SNF 31003A_135598.

Disclosure: **D.K. Schlegel**, None; **S.M.K. Glasauer**, None; **J.M. Mateos**, None; **G. Barmettler**, None; **U. Ziegler**, None; **S.C.F. Neuhauss**, None

References

1. Bech-Hansen NT, Naylor MJ, Maybaum TA, et al. Loss-of-function mutations in a calcium-channel alpha1-subunit gene in Xp11.23 cause incomplete X-linked congenital stationary night blindness. *Nature Genet*. 1998;19:264–267.
2. Strom TM, Nyakatura G, Apfelstedt-Sylla E, et al. An L-type calcium-channel gene mutated in incomplete X-linked congenital stationary night blindness. *Nat Genet*. 1998;19:260–260.
3. Morgans CW. Localization of the alpha(1F) calcium channel subunit in the rat retina. *Invest Ophthalmol Vis Sci*. 2001;42:2414–2418.
4. Mansergh F, Orton NC, Vessey JP, et al. Mutation of the calcium channel gene Cacna1f disrupts calcium signaling, synaptic transmission and cellular organization in mouse retina. *Hum Mol Genet*. 2005;14:3035–3046.
5. Ball SL, Powers PA, Shin H-S, Morgans CW, Peachey NS, Gregg RG. Role of the beta(2) subunit of voltage-dependent calcium channels in the retinal outer plexiform layer. *Invest Ophthalmol Vis Sci*. 2002;43:1595–1603.
6. Wycisk KA, Budde B, Feil S, et al. Structural and functional abnormalities of retinal ribbon synapses due to Cacna2d4 mutation. *Invest Ophthalmol Vis Sci*. 2006;47:3523–3530.
7. Wycisk KA, Zeitz C, Feil S, et al. Mutation in the auxiliary calcium-channel subunit CACNA2D4 causes autosomal recessive cone dystrophy. *Am J Hum Genet*. 2006;79:973–977.
8. Knoflach D, Kerov V, Sartori SB, et al. Cav1.4 IT mouse as model for vision impairment in human congenital stationary night blindness type 2. *Channels (Austin)*. 2013;7:503–513.
9. Lee A, Wang S, Williams B, Hagen J, Scheetz TE, Haeseleer F. Characterization of Cav1.4 complexes (α11.4, β2, and α2δ4) in HEK293T cells and in the retina. *J Biol Chem*. 2015;290:1505–1521.
10. Seitter H, Koschak A. Relevance of tissue specific subunit expression in channelopathies. *Neuropharmacology*. 2018;132:58–70.
11. Mantyjarvi M, Nurmenniemi P, Partanen J, Myohanen T, Peippo M, Alitalo T. Clinical features and a follow-up study in a family with X-linked progressive cone-rod dystrophy. *Acta Ophthalmol Scand*. 2001;79:359–365.
12. Jalkanen R, Mäntyjärvi M, Tobias R, et al. X linked cone-rod dystrophy, CORDX3, is caused by a mutation in the CACNA1F gene. *J Med Genet*. 2006;43:699–704.
13. Huang L, Zhang Q, Li S, et al. Exome sequencing of 47 Chinese families with cone-rod dystrophy: mutations in 25 known causative genes. *PLoS One*. 2013;8:e65546.
14. Hauke J, Schild A, Neugebauer A, et al. A novel large in-frame deletion within the CACNA1F gene associates with a cone-rod dystrophy 3-like phenotype. *PLoS One*. 2013;8:e76414.
15. Jalkanen R, Bech-Hansen NT, Tobias R, et al. A novel CACNA1F gene mutation causes Aland Island eye disease. *Invest Ophthalmol Vis Sci*. 2007;48:2498–502.
16. Nachman-Clewner M, St. Jules R, Townes-Anderson E. L-type calcium channels in the photoreceptor ribbon synapse: Localization and role in plasticity. *J Comp Neurol*. 1999;415:1–16.
17. Chang B, Heckenlively JR, Bayley PR, et al. The nob2 mouse, a null mutation in Cacna1f: anatomical and functional abnormalities in the outer retina and their consequences on ganglion cell visual responses. *Vis Neurosci*. 2006;23:11–24.
18. Zabouri N, Haverkamp S. Calcium channel-dependent molecular maturation of photoreceptor synapses. *PLoS One*. 2013;8:e63853.
19. Liu X, Kerov V, Haeseleer F, et al. Dysregulation of Ca(v)1.4 channels disrupts the maturation of photoreceptor synaptic ribbons in congenital stationary night blindness type 2. *Channels (Austin)*. 2013;7:514–523.
20. Jia S, Muto A, Orisme W, et al. Zebrafish Cacna1fa is required for cone photoreceptor function and synaptic ribbon formation. *Hum Mol Genet*. 2014;23:2981–2994.
21. Dolphin AC. The α2δ subunits of voltage-gated calcium channels. *Biochimica et Biophysica Acta*. 2013;1828:1541–1549.
22. Ba-Abbad R, Arno G, Carss K, et al. Mutations in CACNA2D4 cause distinctive retinal dysfunction in humans. *Ophthalmology*. 2016;123:668–71.e2.
23. Wang Y, Fehlhaber KE, Sarria I, et al. The auxiliary calcium channel subunit α2δ4 is required for axonal elaboration, synaptic transmission, and wiring of rod photoreceptors. *Neuron*. 2017;93:1359–1374.e6.
24. Kerov V, Laird JG, Joiner M-L, et al. α2δ-4 is required for the molecular and structural organization of rod and cone photoreceptor synapses. *J Neurosci*. 2018;38:6145–6160.

Downloaded from iovs.arvojournals.org on 12/16/2019

25. Mullins MC, Hammerschmidt M, Haffter P, Nüsslein-Volhard C. Large-scale mutagenesis in the zebrafish: in search of genes controlling development in a vertebrate. *Curr Biol*. 1994;4:189–202.
26. Kimmel CB, Ballard WW, Kimmel SR, Ullmann B, Schilling TF. Stages of embryonic development of the zebrafish. *Dev Dyn*. 1995;203:253–310.
27. Dereeper A, Guignon V, Blanc G, et al. Phylogeny.fr: robust phylogenetic analysis for the non-specialist. *Nucleic Acids Res*. 2008;36:W465–W469.
28. Dereeper A, Audic S, Claverie J-M, Blanc G. BLAST-EXPLORER helps you building datasets for phylogenetic analysis. *BMC Evol Biol*. 2010;10:8.
29. Pierleoni A, Martelli PL, Casadio R. PredGPI: a GPI-anchor predictor. *BMC Bioinformatics*. 2008;9:392.
30. Thisse C, Thisse B. High-resolution in situ hybridization to whole-mount zebrafish embryos. *Nat Protoc*. 2008;3:59–69.
31. Haug MF, Gesemann M, Mueller T, Neuhauss SCF. Phylogeny and expression divergence of metabotropic glutamate receptor genes in the brain of zebrafish (Danio rerio). *J Comp Neurol*. 2013;521:1533–1560.
32. Gagnon JA, Valen E, Thyme SB, et al. Efficient mutagenesis by Cas9 protein-mediated oligonucleotide insertion and large-scale assessment of single-guide RNAs. *PLoS One*. 2014;9:e98186.
33. Jao L-E, Wente SR, Chen W. Efficient multiplex biallelic zebrafish genome editing using a CRISPR nuclease system. *Proc Natl Acad Sci U S A*. 2013;110:13904–13909.
34. Jinek M, East A, Cheng A, Lin S, Ma E, Doudna J. RNA-programmed genome editing in human cells. *eLife*. 2013;2:e00471.
35. Burger A, Lindsay H, Felker A, et al. Maximizing mutagenesis with solubilized CRISPR-Cas9 ribonucleoprotein complexes. *Development*. 2016;143:2025–2037.
36. Huang Y-Y, Haug MF, Gesemann M, Neuhauss SCF. Novel expression patterns of metabotropic glutamate receptor 6 in the zebrafish nervous system. *PLoS One*. 2012;7:e35256.
37. Mateos JM, Barmettler G, Doehner J, Kaech A, Ziegler U. Direct imaging of uncoated biological samples enables correlation of super-resolution and electron microscopy data. *Sci Rep*. 2018;8:11610.
38. Mateos JM, Barmettler G, Doehner J, et al. Correlative super-resolution and electron microscopy to resolve protein localization in zebrafish retina. *J Vis Exp*. 2017;129:56113.
39. Makhankov YV, Rinner O, Neuhauss SCF. An inexpensive device for non-invasive electroretinography in small aquatic vertebrates. *J Neurosci Methods*. 2004;135:205–210.
40. Niklaus S, Cadetti L, Vom Berg-Maurer CM, et al. Shaping of signal transmission at the photoreceptor synapse by eaat2 glutamate transporters. *eNeuro*. 2017;4:ENEURO.0339-16.2017.
41. Whittaker CA, Hynes RO. Distribution and evolution of von Willebrand/integrin A domains: widely dispersed domains with roles in cell adhesion and elsewhere. *Mol Biol Cell*. 2002;13:3369–3387.
42. Anantharaman V, Aravind L. Cache – a signaling domain common to animal Ca2+-channel subunits and a class of prokaryotic chemotaxis receptors. *Trends Biochem Sciences*. 2000;25:535–537.
43. Branchek T. The development of photoreceptors in the zebrafish, brachydanio rerio. II. Function. *J Comp Neurol*. 1984;224:116–122.
44. Bilotta J, Saszik S, Sutherland SE. Rod contributions to the electroretinogram of the dark-adapted developing zebrafish. *Dev Dyn*. 2001;222:564–5670.
45. Hughes A, Saszik S, Bilotta J, DeMarco PJ, Patterson WF. Cone contributions to the photopic spectral sensitivity of the zebrafish ERG. *Vis Neurosci*. 1998;15:1029–1037.
46. Vincent A, Deshmukh S, Wright T, Sanchez Y-G, Westall CA, Heon E. Non-truncating homozygous deletion in CACNA2D4 mimicking oligocone trichromacy. *Invest Ophthalmol Vis Sci*. 2014;55:6427.
47. Wan L, Almers W, Chen W. Two ribeye genes in teleosts: the role of Ribeye in ribbon formation and bipolar cell development. *J Neurosci*. 2005;25:941–949.
48. Dick O, tom Dieck S, Altrock WD, et al. The presynaptic active zone protein bassoon is essential for photoreceptor ribbon synapse formation in the retina. *Neuron*. 2003;37:775–786.
49. Haeseleer F, Imanishi Y, Maeda T, et al. Essential role of Ca2+-binding protein 4, a Cav1.4 channel regulator, in photoreceptor synaptic function. *Nat Neurosci*. 2004;7:1079–1087.
50. Specht D, tom Dieck S, Ammermüller J, Regus-Leidig H, Gundelfinger ED, Brandstätter JH. Structural and functional remodeling in the retina of a mouse with a photoreceptor synaptopathy: plasticity in the rod and degeneration in the cone system. *Eur J Neurosci*. 2007;26:2506–2515.
51. Hoppa MB, Lana B, Margas W, Dolphin AC, Ryan TA. α2δ expression sets presynaptic calcium channel abundance and release probability. *Nature*. 2012;486:122–125.
52. Cassidy JS, Ferron L, Kadurin I, Pratt WS, Dolphin AC. Functional exofacially tagged N-type calcium channels elucidate the interaction with auxiliary α2δ-1 subunits. *Proc Natl Acad Sci U S A*. 2014;111:8979–8984.
53. Pirone A, Kurt S, Zuccotti A, et al. α2δ3 is essential for normal structure and function of auditory nerve synapses and is a novel candidate for auditory processing disorders. *J Neurosci*. 2014;34:434–445.
54. Xu H-P, Zhao J-W, Yang X-L. Expression of voltage-dependent calcium channel subunits in the rat retina. *Neurosci Lett*. 2002;329:297–300.
55. Katiyar R, Weissgerber P, Roth E, et al. Influence of the β2-subunit of l-type voltage-gated cav channels on the structural and functional development of photoreceptor ribbon synapses. *Invest Ophthalmol Vis Sci*. 2015;56:2312–2324.

Investigative Ophthalmology & Visual Science

Downloaded from iovs.arvojournals.org on 12/16/2019